

Quantum Band Structure and Topology in One Dimensional Modulated Plasmonic Crystal

Luis Brey

Instituto de Ciencia de Materiales de Madrid (CSIC), Cantoblanco, 28049 Madrid, Spain

H.A. Fertig

*Department of Physics, Indiana University, Bloomington, IN 47405 and
Quantum Science and Engineering Center, Indiana University, Bloomington, IN, 47408*

(Dated: October 16, 2024)

Band structures of electrons in a periodic potential are well-known to host topologies that impact their behaviors at edges and interfaces. The concept however is more general than the single-electron setting. In this work, we consider topology of plasmons in a two-dimensional metal, subject to a unidirectional periodicity. We show how the plasmon modes and wavefunctions may be computed for such a periodic system, by focusing on the confined, quantized photon degrees of freedom associated with the plasmon modes. At low frequencies the plasmons disperse with wavevector as \sqrt{q} ; however at higher frequencies one finds a series of bands and gaps in the spectrum. For a unidirectional periodic electron density with inversion symmetry, we show that each band hosts a Zak phase γ_n which may only take the values 0 or π . Each gap has a topological index ν that is determined by the sum of the Zak phases below it. When the system has an interface with the vacuum, one finds in-gap modes for gaps with non-trivial topologies, which are confined to the interface. In addition, interfaces between systems that are the same except for their topologies – which can be created by a defect in the lattice in which half a unit cell has been removed – host in-gap, confined states when the topological indices of the relevant gaps are different. We demonstrate these properties numerically by analyzing a Kronig-Penney-type model in graphene, in which the electron density is piecewise constant, modulating between two different densities. In addition, we consider a related plasmon system modeled after the Su-Schrieffer-Heeger (SSH) model. We show that the topological phase diagram of the lowest energy bands is highly analogous to that of the SSH tight-binding system.

I. INTRODUCTION

Plasmons are collective excitations of an electron gas that appear due to the long-range character of the Coulomb interaction between electrons^{1–5}. When the electrons are confined to move in two-dimensions the plasmons become gapless and disperse as $\sim \sqrt{q}$, where \mathbf{q} is the two-dimensional (2D) momentum^{6–10}. Plasmons in general may be described in different ways. For example, one may focus on the charge degrees of freedom of a conducting system, so that they arise as divergences in its charge density response function, thus corresponding to self-sustained charge density excitations⁴. In 2D electron gases, they can alternatively be understood as electromagnetic waves confined to the vicinity of the electron sheet. In this context, they are also known also as surface-plasmon polaritons^{11–15}. The latter approach is particularly useful for describing coupling of plasmons with atoms^{16,17}, resulting in plasmon-mediated interactions among quantum emitters (as realized by the atomic electronic degrees of freedom)¹⁸. The plasmon-polariton approach is also useful for understanding chemical reactions driven by confined electromagnetic fields¹⁹.

Plasmons confined in graphene are particularly interesting. Their frequencies, which fall within the mid-infrared and terahertz spectral ranges, can be tuned via gating^{20–22}. These plasmons can be directly observed in near-field microscopy experiments^{23–25} and support long

propagation lengths²⁶. Moreover, graphene can be patterned or gated to modulate the density of carriers and create periodic nanostructures in one^{27–35} and two^{36–38} dimensions. These metamaterials, in analogy to photonic crystals³⁹, are referred to as plasmonic crystals. The periodicity induces destructive interference, potentially creating one or more frequency gaps where light cannot propagate.

In analogy with electronic systems⁴⁰, the plasmon band structure of a plasmonic crystal does not contain all the information about the modes. In particular, the topology of the plasmon wave functions can be crucial for understanding the localization behavior of plasmons at defects and interfaces. Topological and geometric effects of the type now well-known for electron bands⁴⁰ have been proposed to occur in plasmonic^{41–43} and photonic crystals^{44–47}.

In graphene, one-dimensional plasmonic crystals can be created by periodically varying a metal-gated structure, or by depositing a periodic metal grating on the graphene sheet. This modulation induces a periodic variation in the carrier density profile, perturbing the plasmons and generating subbands^{33,34,48}. The simplest description of this structure is a Kronig-Penney⁴⁹ (KP) model, consisting of alternating regions with different charge densities. This one-dimensional approach captures the essence of band structure formation in such metamaterials. Most calculations of plasmon band structures in such metamaterials have been performed classi-

cally, matching the electric and magnetic fields at the interfaces between regions with different densities using appropriate boundary conditions^{12,15}.

For non-interacting electrons, a paradigm for topological band structures is the Su-Schrieffer-Heeger (SSH)⁵⁰ model. In its simplest realization, this is a tight-binding structure with two sites per unit cell and two different hopping amplitudes, resulting in two bands which may or may not be topological in nature. Because of its simplicity, most existing work on the topology of one-dimensional crystal plasmons focus on describing the two lowest subbands, mapping the system onto a 2×2 tight-binding SSH-like Hamiltonian^{51–54}. This can be achieved, for example, by building the unit cell to contain two equal regions of high electron density, separated by two unequal regions of low electron density^{51–53}. However, for this mapping to be valid, the energy gap between the second and third subbands should be larger than the gap between the first and second subbands^{55,56} if one wishes to ignore higher energy subbands. In general, a continuous modulation of the density results in the formation of an infinite number of bands separated by similar-sized gaps. Such situations cannot be treated analytically or fully analyzed topologically within the framework of a tight-binding Hamiltonian.

In this work, we present a method for computing the plasmon band structure and wavefunctions of a doped Drude-like graphene layer in the presence of a periodic continuous modulation of the charge density. We apply this method to the case of a one-dimensional KP-like modulation of the Fermi energy. Our focus is on unidirectional plasmonic waveguides, and we analyze in detail plasmons with zero momentum in the direction transverse to the modulations, where one expects to find the lowest energy modes. By calculating the band structure and analyzing the symmetry of the wavefunctions, we determine the Zak phases of the plasmon subbands and the Z_2 topological invariants of the system.

The remainder of this paper is organized as follows. In Section II we present a quantum Hamiltonian that describes plasmons in terms of confined electromagnetic modes, as well as by their periodic modulation of the Fermi energy. In Section III, we explore the plasmon band structure when the graphene Fermi energy exhibits a one-dimensional KP-like modulation. Section IV discusses the Zak phases of the plasmon subbands and their

relationship with the centers of the Wannier functions of these subbands. Additionally, we analyze how the non-trivial topology of the plasmon subbands leads to a topological Z_2 invariant for the system when the energy lies within a subband gap. At the interface between gapped systems with different Z_2 invariants, interface states with energies in the middle of the gap are expected to emerge. In Section V, we demonstrate the existence of such states at the interface between two distinct topological plasmonic crystals, as well as at the interface between a plasmonic crystal and a plasmon vacuum. In Section VI, we examine a KP-like model in which the unit cell consists of two equal regions of high electron density separated by two unequal regions of low density. We demonstrate that this system shows the same topological properties as the SSH model. We conclude in Section VII with a summary of our results.

II. PLASMONIC CRYSTALS.

At long wavelengths and low energies, plasmons in two-dimensional metals depend only on the local optical conductivity $\sigma(\omega; E_F)$ of the electron gas. For frequencies higher than the continuum of the intraband electron-hole pair energies, the metal is essentially dissipationless, and is characterized by a local optical conductivity which for long wavelengths and small frequencies has the Drude-like form^{57–59} $\sigma(\omega; E_F) = i \frac{D}{\omega}$, where $D = \frac{e^2 E_F}{\hbar^2 \pi}$ is the Drude weight and E_F is the Fermi energy. In graphene the band structure disperses linearly with momentum, and the Fermi energy is related to the carrier density, n_0 , by $E_F = \hbar v_D \sqrt{\pi n_0}$, with v_D being the speed of electrons at the graphene Dirac points^{8,60,61}. In the semiclassical limit the plasmon frequency, $\omega_q = \sqrt{\frac{D}{2\epsilon_d \epsilon_0} q}$ (with ϵ_d the dielectric constant of the surrounding medium), is obtained from Maxwell's equations, with proper matching of the fields across the 2D metal sheet^{11,48}.

Such semiclassical plasmons can be quantized in the near-field approximation, which is appropriate when the wavelength of the plasmons is much smaller than that of free light at the same frequency. In this approximation only the longitudinal electric field is considered, and the magnetic field associated with the plasmon mode is neglected. The quantum Hamiltonian describing plasmons in a uniform sheet of a doped metal that emerges from this approach is^{62–67}

$$\hat{H} = \frac{\epsilon_0 \epsilon_d}{2} \int \int d\mathbf{r} dz \hat{\mathbf{E}}(\mathbf{r}, z) \hat{\mathbf{E}}(\mathbf{r}, z) + \frac{1}{2} \int \int d\mathbf{r} dz D \delta(z) \hat{\mathbf{A}}(\mathbf{r}, z) \hat{\mathbf{A}}(\mathbf{r}, z) = \sum_{\mathbf{q}} \frac{\hbar \omega_q}{2} (\hat{a}_{\mathbf{q}} \hat{a}_{\mathbf{q}}^\dagger + \hat{a}_{\mathbf{q}}^\dagger \hat{a}_{\mathbf{q}}), \quad (1)$$

where the operator $\hat{a}_{\mathbf{q}}^\dagger$ creates a plasmon with 2D momentum \mathbf{q} and frequency ω_q . In terms of $\hat{a}_{\mathbf{q}}$, $\hat{a}_{\mathbf{q}}^\dagger$ the

electric field and vector potential operators are

$$\begin{aligned} \hat{\mathbf{E}}(\mathbf{r}, z) &= \sum_{\mathbf{q}} \sqrt{\frac{\hbar \omega_q}{2\epsilon_0 \epsilon_d S}} e^{i\mathbf{q}\mathbf{r}} \mathbf{u}(\mathbf{q}, z) \hat{a}_{\mathbf{q}} + h.c., \\ \hat{\mathbf{A}}(\mathbf{r}, z) &= -i \sum_{\mathbf{q}} \sqrt{\frac{\hbar}{2\epsilon_0 \epsilon_d S \omega_q}} e^{i\mathbf{q}\mathbf{r}} \mathbf{u}(\mathbf{q}, z) \hat{a}_{\mathbf{q}} + h.c., \end{aligned} \quad (2)$$

where S is the sample area and the vectors $\mathbf{u}(\mathbf{q}, z)$ are given by

$$\mathbf{u}(\mathbf{q}, z) = e^{-q|z|} \sqrt{\frac{q}{2}} \left(i \frac{\mathbf{q}}{q} - \frac{z}{|z|} \hat{\mathbf{z}} \right). \quad (3)$$

The first term in Eq. 1 represents the energy stored in the electric field and the second term, which is nonzero only in the conducting layer, is the kinetic energy corresponding to the motion of the charge carriers. The Drude weight represents the stiffness of the electron gas against oscillations.

A non-uniform 2D system is defined by a density of charge that modulates in space. Plasmons in such systems are conventionally studied in a local approximation^{11,14,48,68–72}, that considers the optical conductivity at each point in space to be determined by the local Fermi energy. This in turn is obtained from the local charge density using the Thomas-Fermi approximation⁷³, $\sigma(\mathbf{r}) = \sigma(E_F[n(\mathbf{r})])$, which is im-

plemented by endowing the Drude weight with a spatial dependence. When this dependence is periodic in space, the kinetic energy part of the Hamiltonian Eq.2 is modified by replacing the uniform Drude weight D by

$$D(\mathbf{r}) = D_0 + \delta D(\mathbf{r}) = D_0 + \sum_{\mathbf{G} \neq 0} D_{\mathbf{G}} e^{i\mathbf{G}\mathbf{r}}, \quad (4)$$

where D_0 is the average Drude weight, $\{\mathbf{G}\}$ are the reciprocal lattice vectors associated with the periodicity of the modulation, $D_{\mathbf{G}} = \frac{1}{S_{u.c.}} \int_{u.c.} d^2r D(\mathbf{r}) e^{-i\mathbf{G}\mathbf{r}}$ and $\int_{u.c.} d^2r$ and $S_{u.c.}$ are a unit cell integral and the unit cell area, respectively. Using this form of $D(\mathbf{r})$ and the definition of the vector potential operators as functions of $\hat{a}_{\mathbf{q}}^\dagger$ and $\hat{a}_{\mathbf{q}}$, Eq. 2, one arrives at

$$\hat{H} = \sum_{\mathbf{k}, \mathbf{G}} \hbar \omega_{|\mathbf{k}+\mathbf{G}|} \left(\hat{a}_{\mathbf{k}+\mathbf{G}}^\dagger \hat{a}_{\mathbf{k}+\mathbf{G}} + \frac{1}{2} \right) + \sum_{\mathbf{k}, \mathbf{G}, \mathbf{G}'} \hat{V}(\mathbf{k}+\mathbf{G}, \mathbf{k}+\mathbf{G}'), \quad (5)$$

with

$$\hat{V}(\mathbf{k} + \mathbf{G}, \mathbf{k} + \mathbf{G}') = V(\mathbf{k} + \mathbf{G}, \mathbf{k} + \mathbf{G}') \left(\hat{a}_{\mathbf{k}+\mathbf{G}}^\dagger \hat{a}_{\mathbf{k}+\mathbf{G}'} - \hat{a}_{-\mathbf{k}-\mathbf{G}'} \hat{a}_{\mathbf{k}+\mathbf{G}} + h.c. \right), \quad (6)$$

where

$$V(\mathbf{k} + \mathbf{G}, \mathbf{k} + \mathbf{G}') = \frac{1}{4} \hbar \sqrt{\omega_{|\mathbf{k}+\mathbf{G}|} \omega_{|\mathbf{k}+\mathbf{G}'|}} \frac{(\mathbf{k} + \mathbf{G}) \cdot (\mathbf{k} + \mathbf{G}')}{|\mathbf{k} + \mathbf{G}| |\mathbf{k} + \mathbf{G}'|} \frac{D_{\mathbf{G}-\mathbf{G}'}}{D_0}. \quad (7)$$

In Eq. 5, the momentum \mathbf{k} is restricted to values in the first Brillouin zone associated with the periodicity of the Drude weight. The first term appearing in Eq. 6 is a resonant contribution that describes the transfer of momentum $\mathbf{G} - \mathbf{G}'$ between two plasmons. The second term describes processes which are non-conserving in the number of plasmons, describing the simultaneous annihilation of a pair of plasmons while transferring a momentum $\mathbf{G} - \mathbf{G}'$ to the system. In quantum optics, such non-conserving contributions to the Hamiltonian are known as counterrotating (CR) terms^{17,74–78}. Using this quantum formalism we obtain in a transparent way the scattering between two plasmons with momentum \mathbf{q} and \mathbf{q}' due to density inhomogeneities^{79–83}. The scattering potential of plasmons by a spatial modulation of the Drude weight is formally equivalent to the Rayleigh scattering of phonons by a modulation of the atomic mass⁸⁴.

The Hamiltonian Eq. 5 is bilinear in field operators and can be diagonalized using a Bogoliubov-Hopffield symplectic transformation^{67,85,86}. The transformed Hamiltonian takes the form

$$\hat{H} = \sum_{\mathbf{k}, n} E_{k,n} \left(\hat{b}_{\mathbf{k},n}^\dagger \hat{b}_{\mathbf{k},n} + \frac{1}{2} \right) \quad (8)$$

where $E_{\mathbf{k},n}$ are the energies of the plasmon modes, where here n is a band index. The eigenstates corresponding to a mode \mathbf{k}, n have the form

$$\hat{b}_{n,\mathbf{k}}^\dagger = \sum_{\mathbf{G}} \left(\alpha_{\mathbf{k}+\mathbf{G}}^n \hat{a}_{\mathbf{k}+\mathbf{G}}^\dagger + \beta_{\mathbf{k}+\mathbf{G}}^n \hat{a}_{-\mathbf{k}-\mathbf{G}} \right). \quad (9)$$

The counterrotating terms in Eq. 6 lead to an admixture of creation and annihilation operators of the uniform system forming the operators that create and annihilate normal modes of the periodic system. The operators \hat{b} and \hat{b}^\dagger are bosonic, and order to satisfy the proper commutation relations, the coefficients $\{\alpha\}$ and $\{\beta\}$ must satisfy the conditions

$$\sum_{\mathbf{G}} [(\alpha_{\mathbf{k}+\mathbf{G}}^n)^2 - (\beta_{\mathbf{k}+\mathbf{G}}^n)^2] = 1. \quad (10)$$

Real space wave functions for the crystal plasmons can be cast in a “particle-hole” spinor form,

$$\Psi_{n,\mathbf{k}}(\mathbf{r}) = \begin{pmatrix} \psi_{n,\mathbf{k}}^p(\mathbf{r}) \\ \psi_{n,\mathbf{k}}^h(\mathbf{r}) \end{pmatrix} = \begin{pmatrix} \langle \Phi_0 | \hat{\Psi}(\mathbf{r}) \hat{b}_{n,\mathbf{k}}^\dagger | \Phi_0 \rangle \\ \langle \Phi_0 | \hat{\Psi}^\dagger(\mathbf{r}) \hat{b}_{n,\mathbf{k}}^\dagger | \Phi_0 \rangle \end{pmatrix} = \frac{1}{\sqrt{S}} \begin{pmatrix} \sum_{\mathbf{G}} \alpha_{\mathbf{k}+\mathbf{G}}^n e^{i(\mathbf{k}+\mathbf{G})\cdot\mathbf{r}} \\ - \sum_{\mathbf{G}} \beta_{-\mathbf{k}-\mathbf{G}}^n e^{i(\mathbf{k}+\mathbf{G})\cdot\mathbf{r}} \end{pmatrix}. \quad (11)$$

Here $\hat{\Psi}(\mathbf{r}) = \frac{1}{\sqrt{S}} \sum_{\mathbf{q}} e^{i\mathbf{q}\cdot\mathbf{r}} \hat{a}_{\mathbf{q}}$ is an operator that annihilates a plasmon at location \mathbf{r} , and $|\Phi_0\rangle$ is the vacuum of the plasmonic crystal, defined by $b_{n,\mathbf{k}}|\Phi_0\rangle = 0$, for all n and \mathbf{k} .

The modulation of the Drude weight couples plasmons with momenta \mathbf{q} and $\mathbf{q} + \mathbf{G}$. At the center and edges of the Brillouin zone, unperturbed plasmons with momenta \mathbf{q} and $\mathbf{q} + \mathbf{G}$ become degenerate and thus are strongly coupled by the perturbation^{87–89}. This coupling opens gaps in frequency at which plasmons cannot propagate.

III. ONE-DIMENSIONAL MODULATION.

In this section, we analyze the plasmon band structure of a system with a one-dimensional modulation of the Drude weight of period d . The reciprocal lattice vectors are $G_n = nG_0$, with $G_0 = \frac{2\pi}{d}$ and n an integer, and we write the spatially varying Fermi energy in the form $E_F(x) = \sum_{G_n} E_{F,n} e^{iG_n x}$. As a simple model we analyze a Kronig-Penney model in which regions of width b having a Fermi energy $E_F^{(2)} = E_F + \Delta E_F$ alternate with regions of width $d-b$ having Fermi energy $E_F^{(1)} = E_F - \Delta E_F$. (See Fig. 1.)

Following the strategy described in the previous section, we can obtain the plasmon band structure by diagonalizing the resulting Hamiltonian (Eq. 5.) The white dots in Fig. 1(a) show the result for unit cell parameters $d=100\text{nm}$, $b=50\text{nm}$, $E_F=500\text{meV}$ and $\Delta E_F=250\text{meV}$. To verify the accuracy of this quantum calculation, we also plot the loss function of this system obtained through self-consistent solutions of the Poisson equation, Ohm's law, and the continuity equation. (Details are provided in Appendix A). The agreement is excellent, which is perhaps not surprising since the Hamiltonian Eq. 5 describes a system of coupled harmonic oscillators, for which classical and quantum modes have identical frequencies. In Fig. 1(b) we compare the dispersion of the full Hamiltonian Eq. 5 with what is obtained in the Rotating Wave Approximation (RWA), which consists of neglecting the counter-rotating terms in the Hamiltonian, Eqs. 5-6. The RWA shifts the bands to higher energies, with the shift becoming more significant as the modulation of the Drude weight increases. Throughout the remainder of this work, unless stated to the contrary, we will include the counter-rotating terms in our calculations. Finally, we note that, because the Fermi energy is non-vanishing across the entire unit cell, at low energies the modes disperse as \sqrt{q} , indicating that the periodic modulation has little effect at long wavelengths and low frequencies.

The modulation of the Drude weight creates energy gaps both at the Brillouin zone center [Γ point, $\mathbf{k} = (0, 0)$] and at its edge [M point, $\mathbf{k} = (\frac{G_0}{2}, 0)$]. The gap that separates the two lowest energy subbands occurs at the M point, where the states of the unperturbed system $|\mathbf{k} = -\frac{G_0}{2}\hat{x}\rangle$ and $|\mathbf{k} = \frac{G_0}{2}\hat{x}\rangle$ are degenerate, and are strongly admixed by the modulation of the Drude weight

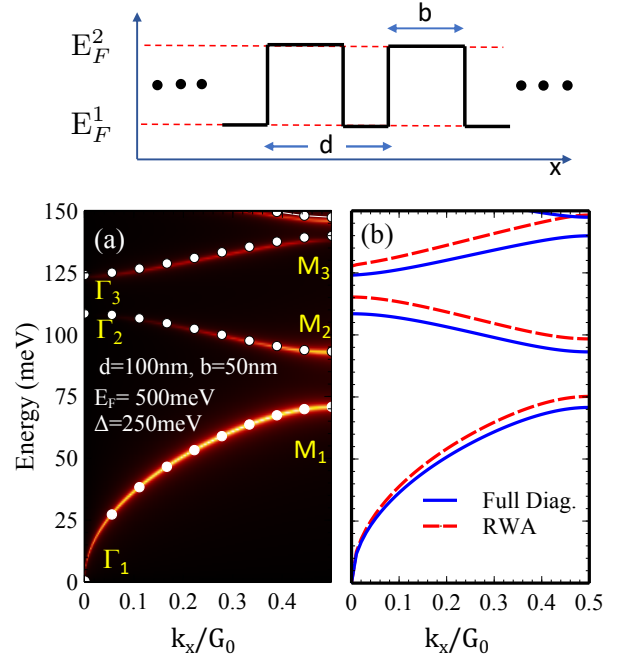


FIG. 1. Upper panel: Schematically diagram of one-dimensional modulation of the Fermi energy in a Kronig-Penney model. Bottom panels: Plasmon band structure for a 1D modulation of period $d=100\text{nm}$. The unit cell consists of two equal regions with Fermi energies $E_F^{(1)}=250\text{meV}$ and $E_F^{(2)}=750\text{meV}$, and dielectric constant $\epsilon_d=5$. In (a), the white points correspond to the dispersion obtained by diagonalizing Eq. 5. The color plot indicates the loss function of the same system as obtained semi-classically. In (b) we compare the dispersion obtained by diagonalizing the full Hamiltonian Eq. 5 with that obtained in the RWA, which neglects terms that are non-conserving in plasmon number. The states denoted as Γ_n and M_n represent the n^{th} state at the Γ and M points, respectively.

(see Eq. 7.) To linear order in V , the lowest energy crystal plasmon modes at the M point may be obtained by evaluating Eq. 5 in the subspace of these two (unperturbed) states. This results in the effective 2×2 effective Hamiltonian⁸⁸

$$H = \begin{pmatrix} \hbar\omega_{\frac{G_0}{2}} & 0 \\ 0 & \hbar\omega_{\frac{G_0}{2}} \end{pmatrix} + \begin{pmatrix} 0 & -\frac{1}{4}\hbar\omega_{\frac{G_0}{2}} \left(\frac{E_{F,1}}{E_{F,0}} \right) \\ -\frac{1}{4}\hbar\omega_{\frac{G_0}{2}} \left(\frac{E_{F,1}}{E_{F,0}} \right) & 0 \end{pmatrix}. \quad (12)$$

The eigenvalues of Eq. 12 are

$$\hbar\omega_{\pm} = \hbar\omega_{\frac{G_0}{2}} \left(1 \pm \frac{1}{4} \left| \frac{E_{F,1}}{E_{F,0}} \right| \right),$$

and its eigenvectors are

$$|\Psi_{\pm, M}\rangle = \frac{1}{\sqrt{2}} \left(|\mathbf{k} = -\frac{G_0}{2}\hat{x}\rangle \mp \text{sgn}(E_{F,1}) |\mathbf{k} = \frac{G_0}{2}\hat{x}\rangle \right).$$

Note that while the energy gap is independent of the sign of $E_{F,1}$, the parity of the wave function depends upon it.

This fact plays a role in the band topology, as we now discuss.

IV. ZAK PHASE IN ONE-DIMENSIONAL PLASMONIC CRYSTALS.

The band structure of electrons in a crystal by itself does not contain all the information about the electronic structure and the accompanying electron dynamics in the system. Modern band theory shows that the *topology* of electron states is also necessary for understanding and predicting various properties. In particular, for one-dimensional systems, the presence of localized states at defects and sample boundaries depends on this topology^{40,90}.

The topological content of energy bands can often be expressed in terms of Berry phases. Quite generally, the Berry phase is a geometrical global phase that a quantum state vector, specified by some set of parameters, accumulates as it is adiabatically transported around a closed path in the parameter space. In band theory the relevant vector spaces consist of the Bloch wave functions, and the parameter space is formed by the wavevectors themselves⁴⁰. However, the calculation of Berry phases involves computing inner products of wave functions at different wavevectors, for which the relevant inner products of the Bloch wavefunctions $\langle \Psi_{n,\mathbf{k}_1} | \Psi_{n,\mathbf{k}_2} \rangle$ vanish for $\mathbf{k}_1 \neq \mathbf{k}_2$ but not for $\mathbf{k}_1 = \mathbf{k}_2$. This means they do not have the smoothness needed to reveal phase changes along a continuous path in momentum space. However, this property *is* present for spinor-like cell-periodic functions $U_{n,\mathbf{k}}(\mathbf{r}) = e^{-i\mathbf{k}\cdot\mathbf{r}} \Psi_{n,\mathbf{k}}(\mathbf{r})$. The improved behavior results from the fact that these functions satisfy the same boundary conditions for all wavevectors \mathbf{k} , so that they may be mapped to a single Hilbert space in which states evolve smoothly with \mathbf{k} .

In one-dimensional systems, the Berry phase acquired by wavefunctions of an isolated band, n , as the wavevector k adiabatically evolves through the entire Brillouin zone, is known as the Zak phase^{91,92}. In electronic tight-binding systems, the scalar inner product of the wave functions that are needed to compute the Zak phase have the form $V_{n,k}^\dagger \cdot V_{n,k'}$, where the entries of $V_{n,k}$ are associated with amplitudes for an electron to be in different orbitals/sites. Here we are interested in finding a corresponding expression for the Zak phase for plasmons in a one-dimensional crystal structure. Because the plasmon states correspond to coherent admixtures of *bosonic* operators that add and remove plasmons from the corresponding uniform system, the needed inner products should be modified^{93,94} to $\langle U_{n,k} | \sigma_z | U_{n,k'} \rangle$ (see Eq. 10.) Note that the scalar product in this expression involves an integral over a single unit cell. The Zak phase of an isolated band in a plasmonic crystal then takes the form

$$\gamma_n = i \int_{-\frac{\pi}{d}}^{\frac{\pi}{d}} dk \langle U_{n,k} | \sigma_z | \partial_k U_{n,k} \rangle. \quad (13)$$

In further analogy with electron systems, it is possible to define Wannier functions for isolated plasmonic bands through the relation $w_{n,X}(x) = \frac{d}{2\pi} \int_{-\frac{\pi}{d}}^{\frac{\pi}{d}} e^{-ikX} \Psi_{n,k} dk$, where the allowed values of X are the unit cell centers of the crystal. The location of the Wannier center in the $X = 0$ unit cell of an isolated band is then given by

$$\bar{x}_n = \int_{-\frac{d}{2}}^{\frac{d}{2}} dx w_{n,X=0}^\dagger(x) \sigma_z x w_{n,X=0}(x), \quad (14)$$

and is proportional to the Zak phase of the isolated band n ,

$$\bar{x}_n = \frac{d}{2\pi} \gamma_n. \quad (15)$$

In general, both the Zak phase and the Wannier center can assume any value. However, if the system possesses spatial inversion symmetry, constraints on the Wannier center emerge that are topological in nature. For one-dimensional periodic potentials such as we consider, inversion-symmetric systems always have two inequivalent inversion centers, and the Hamiltonian will be inversion-symmetric when one of these is at the origin ($x = 0$), in which case the other is at the unit cell edge ($x = d/2$). In analogy with the corresponding electron system⁹¹, the plasmon Wannier functions must be centered at one of these points, so that \bar{x}_n can only take the values 0 or $d/2$. Therefore, in a plasmon crystal whose Hamiltonian has spatial inversion symmetry, the Zak phase is a topological index which can only have the values 0 or π . Importantly, *which* of these values a given band takes depends on which of the inversion symmetric points is located at the origin. Because of this, each isolated band n may have one of two different topological characters, $\gamma_n = 0$ or $\gamma_n = \pi$. In what follows we label these two topologies D_1 and D_2 , respectively. For concreteness, in our system (the Kronig-Penney plasmonic crystal), we take D_1 to correspond to taking the origin at the center of the region with higher Fermi energy, whereas in D_2 , the origin is taken at the center of the region with lower Fermi energy.

In systems with spatial inversion symmetry, Zak phases turn out to be related in a simple way to the parity of the wavefunctions at high symmetry points of the Brillouin zone. Specifically, one may show⁹⁵⁻⁹⁷

$$e^{i\gamma_n} = \xi_n(\Gamma) \xi_n(M), \quad (16)$$

where $\xi_n(\mathbf{k})$ represents the parity of the wavefunction $\Psi_{n,\mathbf{k}}$ at wavevector \mathbf{k} , and Γ and M are the time reversal invariant momenta for this system. We demonstrate Eq. 16 in Appendix B. More globally, for a gap between subbands n and $n+1$, one may construct^{40,98} a Z_2 topological invariant, ν , which depends on the Zak phases of the bands with band indices less than or equal to n and is defined as

$$(-1)^\nu = \prod_{i \leq n} \xi_i(\Gamma) \xi_i(M) \quad (17)$$

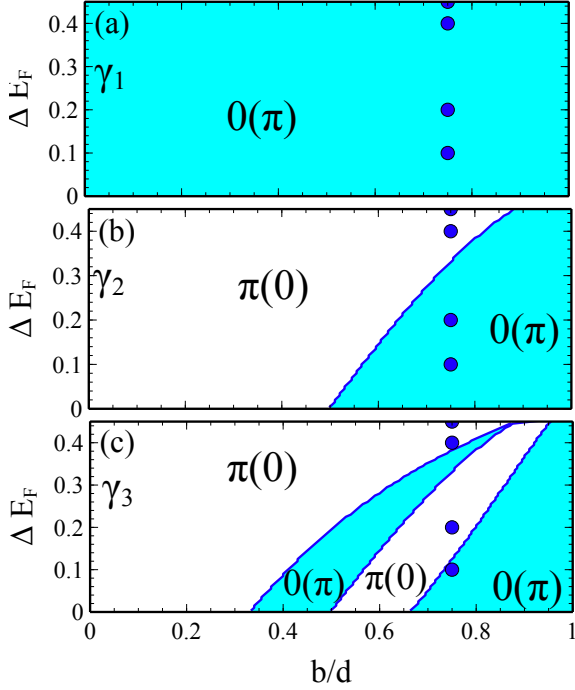


FIG. 2. Zak phases of the three lowest energy subbands: (a) γ_1 , (b) γ_2 and (c) γ_3 , for a Kronig-Penney like model (see Fig. 1) with $d=100\text{nm}$, $E_F=500\text{meV}$ and different values of b/d and ΔE_F . $E_F^{(1,2)}=E_F \pm \Delta E_F$. The phases correspond to topology D_1 . The Zak phases corresponding to topology D_2 are shown in parentheses. The band structure of the points marked in blue are shown in Fig. 3.

As we shall see, these topological invariants dictate the behavior of the spectrum when a system is cut at an inversion-symmetric point, and when there is an interface between systems of D_1 and D_2 topology.

Fig. 2 illustrates the Zak phases of the three lowest energy subbands in the D_1 and D_2 topologies for different values of the Kronig Penney lattice parameters. To understand this behavior, in Fig. 3 we plot the band structure and the parity at the Γ and M wavevectors, for the points marked in blue in Fig. 2. Since the D_1 and D_2 topologies correspond to locating the center of coordinates at different points within the unit cell, the subband Zak phases have opposite values in these states, as required by Eq. 15. The Zak phase of the lowest energy subband in the topology D_1 (D_2) takes the value $\gamma_1 = 0$ (π) across the entire range of parameters studied. In contrast, higher energy subbands exhibit transitions between different values of the Zak phases as the parameters of the Kronig-Penney lattices vary.

In the range of parameters we study, the lowest energy mode disperse from the Γ point ($k = 0$) along the superlattice axis direction as \sqrt{k} , indicating that the main contribution to the plasmon wavefunction, Eq. 11 corresponds to $\mathbf{G}=0$, and the plasmons propagate as a plane

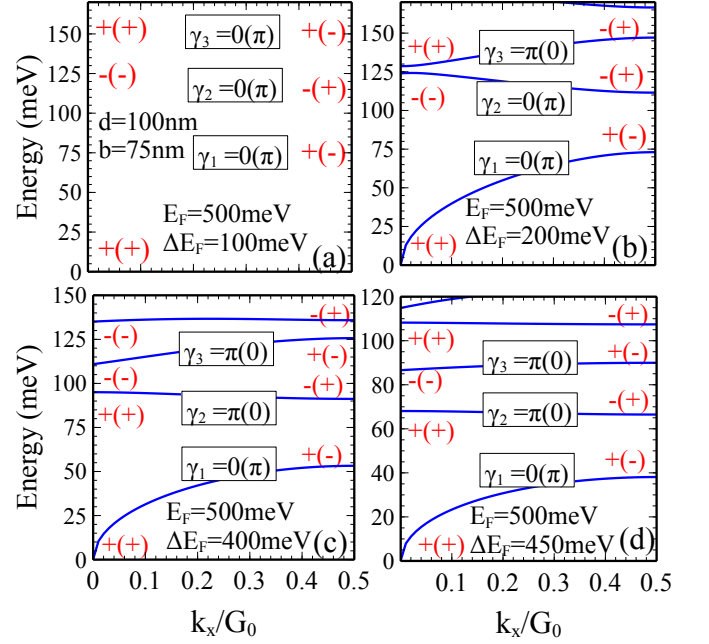


FIG. 3. Plasmon band structures for a Kronig-Penney like model (see Fig. 1), with $d=100\text{nm}$, $b=75\text{nm}$ and different values of $E_F^{(1)}$ and $E_F^{(2)}$, corresponding to the blue points marked in Fig. 2. The parities of the wavefunctions for different plasmon subbands at the points Γ and M are indicated in red. We also show the Zak phase of the different subbands as obtained from Eq. 16. The values without/with parenthesis correspond to topologies D_1 and D_2 , respectively.

wave, e^{ikx} , along the superlattice axis, and the parity of the state at the Γ point is always 1. Thus the Zak phase of the lowest energy subband is determined by the parity of the state at X point, which in turn is fixed by the sign of the potential mixing the unperturbed plasmon states at momenta $-G_0/2$ and $G_0/2$ (see Eq. 12.) In the topologies D_1 and D_2 , the origin of coordinates is located at the maximum and minimum of the Fermi energy, respectively. Therefore, for D_1 the sign of the Fourier component $E_{F,1}$ is positive, while for D_2 it is negative. It follows that the parity of the lowest subband state at the M point is positive in the D_1 topology, and is negative for D_2 . As a consequence, the Zak phase of the lowest energy subband, γ_1 , is zero for D_1 (unit cell centered at maximum of the Fermi energy), and is π for D_2 (unit cell centered at minimum of Fermi energy.)

For weak Fermi energy modulation, the parities of the states at the Γ and M points for the second subband are given by the signs of $E_{F,1}$ and $-E_{F,2}$, respectively. From Eq. 16, this implies $e^{i\gamma_2} = -\text{sgn}(E_{F,1}E_{F,2})$. This suggests a Zak phase transition at $b/d=1/2$, independent of ΔE_F . However, as illustrated in Fig. 2, this only occurs for $\Delta E_F \rightarrow 0$. The discrepancy arises because the coupling to higher energy states results in a crossing of subbands from high energies at the Γ point. (Note, for example,

the exchange of parities for states at the Γ point for the second and third subbands, Γ_2 and Γ_3 , in Fig. 3(b)-(c).) This endows the Zak phase boundary in Fig. 2(b) with a non-trivial b/d dependence. The topology of the third band, γ_3 , depends on the parities of the wavefunctions at Γ_3 and M_3 . Similar to the case of the second subband, under weak modulation, these parities are given by the signs of the Fourier components of the Fermi energy that create the gaps, so that one expects $e^{i\gamma_3} = -\text{sgn}(E_{F,2}E_{F,3})$ for small ΔE . This induces Zak phase transitions at values of $b/d=1/3, 1/2$ and $2/3$. Again, as the value of ΔE_F increases, the coupling with higher energy plasmon states becomes important, moving the Zak phase transitions to larger values of b/d .

V. EDGE AND INTERFACE GAP STATES.

A. Edge States.

A fundamental property of systems with non-trivial topology is the appearance of in-gap states localized at a boundary of the system. In the present context, the topological state associated with a given gap is characterized by a Z_2 topological index, Eq. 17. Such topological indices are very stable against small modifications of the bands (provided the underlying Hamiltonian still retains inversion symmetry). Changes to the topological index occur through topological phase transitions, which occur when gaps in the band structure close. When the system has a boundary, there can effectively be an abrupt change as one moves from the sample interior into the vacuum, for which there are no accessible states, making it effectively topologically trivial. The change of a topological invariant at an edge induces the in-gap states^{50,99}.

In the case of plasmonic crystals the vacuum corresponds to a region with zero Fermi energy, which does not support plasmons. An interface between a plasmonic crystal and empty space may be simulated using a superlattice in which each unit cell includes a slab containing many unit cells of the plasmonic crystal, alongside a wide region with zero Fermi energy. Both the slab and the vacuum region should be sufficiently wide to minimize coupling between states at the edges.

Fig. 4(a) and Fig.4(b) illustrate the energy levels of a superlattice, with unit cell containing 50 unit cells of the plasmonic crystal with $d = 100\text{nm}$ in the topologies D_2 and D_1 respectively, with an adjacent region of zero Fermi energy 5000nm wide. Note that in these systems, the topology is dictated by the form of the E_F profile at the edge, which drops to zero at an inversion symmetry center of the Hamiltonian for the corresponding infinite system. Figures 4(c) and (d) show the Fermi energy profile at the interface of a KP-like plasmonic crystal in topologies D_1 and D_2 (respectively) and the vacuum.

In Fig.4(a), in the lowest energy gap, two states emerge, each corresponding to one of the two boundaries within the unit cell. These two states are not fully degen-

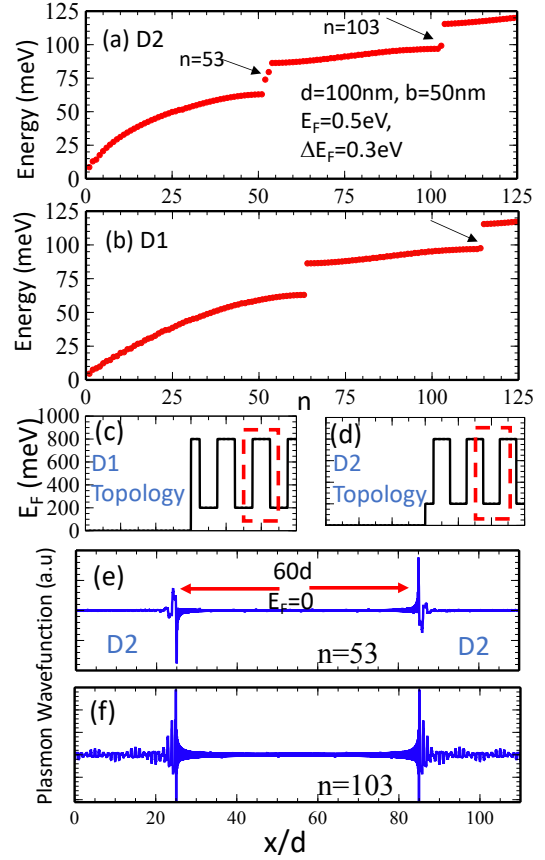


FIG. 4. (a) Energy spectrum of a superlattice with a unit cell consisting of 50 unit cells $d = 100\text{nm}$ of a KP-like plasmonic crystal in the D_2 topology, separated by a region with zero Fermi energy that is 6000 nm wide. The other parameters of the system are indicated in the figure. (b) Same as (a) but for the plasmon superlattice in the state D_1 . (c) and (d): Fermi energy profile at the interface between the region with zero Fermi energy and the KP plasmonic crystal in the D_1 and D_2 topologies, respectively. The unit cells for D_1 and D_2 are highlighted by a red rectangle. (e) Plasmon wave function corresponding to the state $n=53$ that appears inside the first energy gap in (a). (f): Plasmon wave function for the state $n=103$, which appears in the second gap in (a).

erate because the finite size of the superlattice unit cell allows non-negligible interaction between the edge states. These states arise because the Z_2 topological invariant in the first energy gap in the D_2 phase is 1, in contrast with the vacuum space that is topologically trivial (topological invariant 0). The wavefunctions of the in-gap states are localized at the edge of the sample. This is illustrated in Fig. 4(e), which shows the plasmon wave function corresponding to one of the states in the gap. In the second energy gap one also finds a state. This arises due to the difference in the Z_2 invariant between the second gap of the D_2 topology, which remains at 1, and the vanishing topological invariant of the vacuum. Only one state is visible in this gap due to the significant interaction between states localized at different edges. This causes a

large enough level repulsion to shift one of the states into the continuum. The effect is evident in Fig. 4(f), where the plasmon wave function of the state in the second energy gap is illustrated, and has significant weight in the plasmonic crystal region.

In the topology D_1 of the plasmonic crystal, the lowest energy subband hosts trivial topology, and no states appear in the lowest energy gap at the boundary of the crystal, as shown in Fig. 4(b). However, in the D_1 topology, the Zak phase of the second subband is π , leading to the emergence of a state in the second gap. Note for the parameters used in the calculation, this resides barely outside the continuum.

B. Interface States.

States in the gap not only emerge at the boundary of a finite-size insulator with non-trivial topology but also at the interface between two insulators with different topological invariants ν . In this realization, such an interface arises when system is cut at two different inversion points, the finite segment removed, and the remaining semi-infinite systems are stitched together.

To demonstrate this, we performed calculations on a superlattice with a large unit cell composed of 40 unit cells of a KP plasmonic crystal with $d = 100\text{nm}$ in the D_1 topology, and another with 40 unit cells in the D_2 topology. Fig. 5(c) shows the resulting interface, as well as the unit cells of both topologies. In the spectrum of the large superlattice, plasmon states appear in the gaps between the first and second subbands, and between the third and fourth subbands, while no in-gap states appear between the second and third subbands.

This can be understood by examining the band structure of the KP-like plasmonic crystal shown in Fig. 5(b). When the energy gap is between the first and second subbands, the Z_2 topological indices are $\nu_1 = 0$ for D_1 and $\nu_1 = 1$ for D_2 . This change in the Z_2 topological invariant leads to the appearance of plasmon states within the gap. Similarly, for the gap between the third and fourth subbands, the Z_2 topological invariants are also opposite: $\nu_3 = 1$ for D_1 and $\nu_3 = 0$ for D_2 . This difference in topological indices leads to the appearance of in-gap plasmon states as well. Conversely, for the gap between the second and third subbands, both D_1 and D_2 share the same Z_2 topological invariant, $\nu_2 = 1$. In this case, there is no change in topology at the interface, and no edge states appear.

VI. SU-SCHRIEFFER-HEEGER PLASMONIC CRYSTAL.

The Su-Schrieffer-Heeger (SSH) Hamiltonian was introduced to describe the transport properties of polyacetylene through the motion of solitonic defects^{50,100}, and serves as a paradigm^{101–105} for topology in condensed

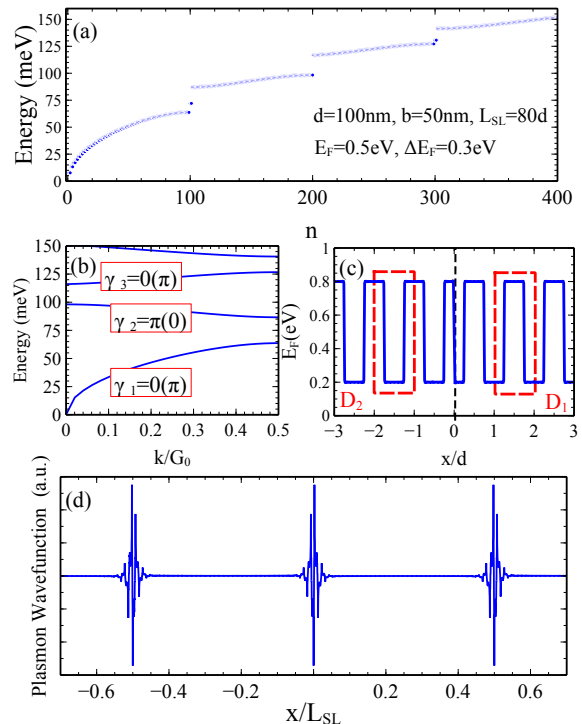


FIG. 5. (a) The energy spectrum as a function of eigenstate number for a superlattice with a unit cell composed of 40 periods of a KP-like plasmonic crystal in the D_1 topology and another 40 periods in the D_2 topology. The unit cell of the supercell is $L_{SL} = 80d$. In-gap states appear in the first and third gaps but not in the second gap. (b) Band structure for the plasmonic crystal and subband Zak phases in the D_1 state. The Zak phases for the D_2 state are shown in parentheses. (c) Interface between the D_1 and D_2 topologies, with the unit cells of both highlighted in red. (d) Plasmon wavefunction for an interface state within the first gap. The parameters of the KP-like plasmonic crystal are displayed in the inset of (a).

matter systems. Experiments across different systems have confirmed some of the topological properties predicted for the SSH model^{106–109}.

The SSH model is a tight-binding Hamiltonian containing two identical atoms per unit cell, with two alternating hopping parameters, t_1 and t_2 . The system has spatial inversion symmetry with symmetry points located at the centers of the two bonds. The electronic spectrum consists of two bands separated by a gap proportional to the difference $t_1 - t_2$. The Wannier centers of the bands are located in the middle of the bond with the largest hopping parameter, t_1 . The system exhibits two non-identical topologies, depending on how the inversion symmetry is realized in the Hamiltonian: either the parameter t_1 or t_2 may describe inter-site hopping within a unit cell, which

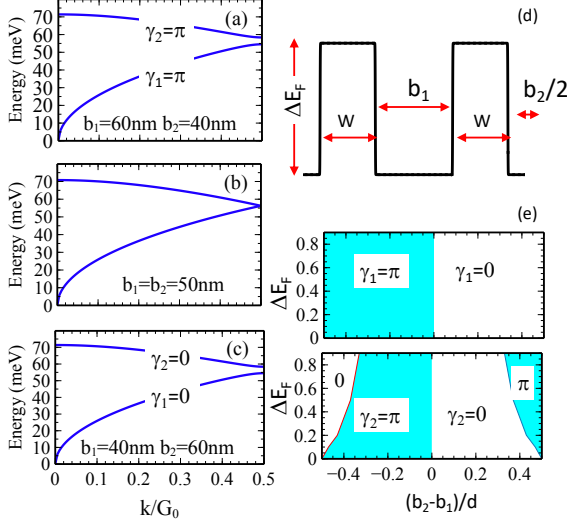


FIG. 6. (a)-(c) Plasmon band structures and subband Zak phases for a SSH-like plasmonic crystal, with unit cell shown schematically in (d). In (b), $b_1=b_2$ and there is no gap between the subbands. (a) and (c) display the bands for positive and negative values of $b_1 - b_2$, respectively. The band energies are identical but their topologies are opposite. (e) Zak phases of the two lowest energy plasmon bands as functions of $b_1 - b_2$ and ΔE_F . Parameters used in these calculations are $d = 200\text{nm}$, $W = 500\text{nm}$, $b_1 + b_2 = 100\text{nm}$, $E_F = 0.5\text{eV}$. For the band structures (a)-(c), $\Delta E_F = 0.25\text{meV}$.

is analogous to choosing which inversion center is used to realize inversion symmetry in the Hamiltonian. For topology D_1 , this intra-cell hopping parameter is chosen to be the larger of the two (t_1), and the bands have Zak phases equal to zero. Topology D_2 , the intra-cell hopping is t_2 , and the Wannier center is effectively shifted to the unit cell edge, which the t_1 hopping effectively crosses. In this case the Zak phases of the bands are π .

For plasmons, an SSH model can be simulated with a unit cell containing two equal regions of width W and Fermi energy $E_F + \Delta E_F$, separated by alternating regions of lower Fermi energy, $E_F - \Delta E_F$ and thickness b_1 and b_2 (see Fig.6(d).) In an analogy with a single particle problem, the regions with the higher Fermi energy act as “wells” for the plasmons, while the regions with lower Fermi energy serve as “barriers”. The coupling between the high Fermi energy regions decreases as the barrier thickness increases, and vice versa. In this way, the difference $b_1 - b_2$ is analogous to the difference $t_1 - t_2$ in the SSH tight-binding model.

Fig. 6(e) shows the Zak phases for the SSH-like plasmonic crystal as a function of $b_2 - b_1$ and ΔE_F . In the calculation, the origin of the unit cell is located at the midpoint of the region with low Fermi energy and width b_1 . Except for very large values of $|b_2 - b_1|$ and ΔE_F , the Zak phase diagram is similar to that of the SSH tight-binding model. When $b_2 > b_1$ the Wannier center is located at the center of the unit cell, $\bar{x}=0$, and the Zak

phases of the lowest energy subbands are zero. By contrast, for negative values of $b_2 - b_1$ the Wannier center is located in the region with width b_2 , and the Zak phases are π for both subbands. A topological phase transition occurs at the line defined by $b_2 = b_1$. Figures 6 (a)-(c) present the plasmon bands energies and Zak phases for $b_2 - b_1$ values less than zero, equal to zero and greater than zero, respectively. A topological phase transition occurs as $b_2 - b_1$ changes sign, with the energy bands crossing and the associated gap closing when $b_2 = b_1$, as expected.

The topology of the SSH-like plasmonic crystals can be understood in terms of the first two Fourier components of the Fermi energy,

$$E_{F,1} = -\frac{\Delta E_F}{\pi} \left(\sin \frac{\pi}{d} b_1 - \sin \frac{\pi}{d} b_2 \right),$$

$$E_{F,2} = -\frac{\Delta E_F}{\pi} \left(\sin \frac{2\pi}{d} b_1 + \sin \frac{2\pi}{d} b_2 \right). \quad (18)$$

As discussed in Section IV, for moderate values of ΔE_F the Zak phases of the lowest energy subbands are $e^{i\gamma_1} = \text{sgn}(E_{F,1})$ and $e^{i\gamma_2} = -\text{sgn}(E_{F,1} E_{F,2})$. Combining these expressions with the forms of $E_{F,1}$ and $E_{F,2}$, one finds precisely the topologies for bands of the SSH-like plasmonic crystal described above, with other low-energy subbands having the same Zak phase.

VII. SUMMARY

Starting from the quantization of plasmons in Drude-like doped graphene, we have constructed a Hamiltonian that describes the coupling among quantum plasmons with different momenta, driven by a periodic modulation of carrier density in the graphene sheet. The Hamiltonian contains terms that describe the scattering of plasmons due to the modulation, as well as non-conserving terms that involve the creation or annihilation of plasmon pairs. We have diagonalized this Hamiltonian for the case of a one-dimensional modulation, and, because we are interested in unidirectional plasmonic waveguides, only focused on plasmons with vanishing momentum transverse to the modulations, $k_y=0$. The modulation creates energy bands and gaps that are proportional to the Fourier components of the Fermi energy modulation.

When the modulation possesses spatial inversion symmetry, and the Hamiltonian is written in an inversion-symmetric way, the topology of each plasmon band is characterized by a Zak phase, 0 or π . This is connected to the center of mass of the band Wannier functions, which lie at center or edge of the real space unit cell, respectively. In a Kronig-Penney-like modulation of the Fermi energy, we find that the Wannier function of the lowest energy plasmon band is centered in the region with higher carrier density. Therefore, when the origin of coordinates in the Hamiltonian is located at this point, and the first Fourier component of the Fermi energy modulation, $E_{F,1}$ is positive, the Zak phase of the lowest en-

ergy band is 0, indicating it is topologically trivial state. However, if the origin is placed at the center of the lower density region, and $E_{F,1}$ is negative, the band acquires a non-trivial topology, with the Zak phase equal to π . Thus, in systems with inversion symmetry, the topological state of the lowest energy sub-band is determined by the sign of the first Fourier component of the Fermi energy modulation. By contrast, for higher energy plasmon sub-bands, the gaps and band topologies depend on higher order Fourier components of the Fermi energy. By varying the modulation of the Fermi energy or the ratio between the linear sizes of the high and low density regions, one may drive multiple transitions between different topological states.

A topological Z_2 invariant can be defined at energies within the gap between two subbands. This invariant is either zero or one, depending on whether the sum of the Zak phases of the lower energy subbands is an even or odd multiple of π . An important property of band topology is that in-gap states should appear at the interface between two topological states with different topological Z_2 invariants. We verified this property by computing the plasmon states at an interface between two systems with the same Kronig-Penney modulation of the Fermi energy, but with unit cells centered either in the higher or lower Fermi energy regions, respectively. We also found in-gap states at the interface between a system with Kronig-Penney modulation of the Fermi energy and a non-metallic region.

Finally, we studied a Kronig-Penney superlattice with a unit cell that simulates an SSH system. The unit cell consists of two equal high-density regions, alternating with low-density regions of different lengths. We find that the topological states of this plasmonic crystal are highly analogous to those of the SSH model.

Acknowledgements – LB was supported by Grant PID2021-125343NB-I00 (MCIN/AEI/FEDER, EU). HAF acknowledges the support of the NSF through Grant No. DMR-1914451, and thanks the Aspen Center for Physics (NSF Grant No. PHY-2210452) for its hospitality.

Appendix A: Semiclassical calculation of plasmons in a 2D electron gas with periodic modulated conductivity.

In this Appendix, we derive the plasmon spectrum for a two-dimensional system with optical conductivity that is periodic in real space,

$$\sigma(\mathbf{r}, \omega) = \sum_{\mathbf{G}} \sigma(\mathbf{G}, \omega) e^{i\mathbf{G}\cdot\mathbf{r}}. \quad (\text{A1})$$

Suppose an external potential acts on the layer,

$$\phi_{ext}(\mathbf{r}, \omega) = e^{i\mathbf{q}\cdot\mathbf{r}} \sum_{\mathbf{G}} \phi_{ext}(\mathbf{q} + \mathbf{G}, \omega) e^{i\mathbf{G}\cdot\mathbf{r}}. \quad (\text{A2})$$

The system screens this potential, creating density oscillations in the layer, $\rho(\mathbf{q} + \mathbf{G}, \omega)$. This in turn induces an electrical potential of the form

$$\phi_{ind}(\mathbf{q} + \mathbf{G}, \omega) = v(|\mathbf{q} + \mathbf{G}|) \rho(\mathbf{q} + \mathbf{G}, \omega), \quad (\text{A3})$$

where $v(q) = 2\pi e / \epsilon_0 \epsilon_d q$. The current in the system responds to the total electric field,

$$\mathbf{J}(\mathbf{r}, \omega) = \sigma(\mathbf{r}, \omega) [\mathbf{E}_{ext}(\mathbf{r}, \omega) + \mathbf{E}_{ind}(\mathbf{r}, \omega)], \quad (\text{A4})$$

where we have assumed a purely local response to the electric field, and an isotropic, scalar conductivity. Writing this equation in reciprocal space yields

$$\begin{aligned} \mathbf{J}(\mathbf{q} + \mathbf{G}, \omega) = & -i \sum_{\mathbf{G}'} (\mathbf{q} + \mathbf{G}') \sigma(\mathbf{G} - \mathbf{G}', \omega) \\ & \times (\phi_{ext}(\mathbf{q} + \mathbf{G}', \omega) + \phi_{ind}(\mathbf{q} + \mathbf{G}', \omega)). \end{aligned} \quad (\text{A5})$$

Combining the continuity equation in reciprocal space,

$$(\mathbf{q} + \mathbf{G}) \cdot \mathbf{J}(\mathbf{q} + \mathbf{G}, \omega) = \omega \rho(\mathbf{q} + \mathbf{G}, \omega), \quad (\text{A6})$$

with Eqs. A3 and A5 yields

$$\begin{aligned} \phi_{ind}(\mathbf{q} + \mathbf{G}, \omega) = & -\frac{i}{\omega} v(|\mathbf{q} + \mathbf{G}|) \sum_{\mathbf{G}'} (\mathbf{q} + \mathbf{G}) \cdot (\mathbf{q} + \mathbf{G}') \\ & \times \sigma(\mathbf{G} - \mathbf{G}') [\phi_{ind}(\mathbf{q} + \mathbf{G}', \omega) + \phi_{ext}(\mathbf{q} + \mathbf{G}', \omega)]. \end{aligned}$$

This implies

$$\begin{aligned} \phi_{tot}(\mathbf{q} + \mathbf{G}, \omega) = & \phi_{ext}(\mathbf{q} + \mathbf{G}, \omega) - \frac{i}{\omega} v(|\mathbf{q} + \mathbf{G}|) \\ & \times \sum_{\mathbf{G}'} (\mathbf{q} + \mathbf{G}) \cdot (\mathbf{q} + \mathbf{G}') \sigma(\mathbf{G} - \mathbf{G}') \phi_{tot}(\mathbf{q} + \mathbf{G}', \omega), \end{aligned}$$

where $\phi_{tot}^T(\mathbf{q} + \mathbf{G}, \omega) = \phi_{ind}(\mathbf{q} + \mathbf{G}, \omega) + \phi_{ext}(\mathbf{q} + \mathbf{G}, \omega)$ is the total electric potential in the system. This equation defines a dielectric matrix (with reciprocal lattice vectors acting as the matrix indices) for the system,

$$\begin{aligned} \epsilon(\mathbf{q} + \mathbf{G}, \mathbf{q} + \mathbf{G}') = & \delta_{\mathbf{q}+\mathbf{G}, \mathbf{q}+\mathbf{G}'} \\ & + \frac{i}{\omega} v(|\mathbf{q} + \mathbf{G}|) (\mathbf{q} + \mathbf{G}) \cdot (\mathbf{q} + \mathbf{G}') \sigma(\mathbf{G} - \mathbf{G}') \end{aligned}$$

Zero eigenvalues of the dielectric matrix determine the plasmon frequencies as functions of q .

In the case of Drude-like metals, where the optical conductivity has the form $\sigma(\mathbf{r}, \omega) = i \frac{D(\mathbf{r})}{\omega}$, the dielectric constant takes the form

$$\epsilon(\mathbf{q} + \mathbf{G}, \mathbf{q} + \mathbf{G}') = \delta_{\mathbf{q}+\mathbf{G}, \mathbf{q}+\mathbf{G}'} - \frac{1}{\omega^2} M(\mathbf{q} + \mathbf{G}, \mathbf{q} + \mathbf{G}'),$$

with

$$M(\mathbf{q} + \mathbf{G}, \mathbf{q} + \mathbf{G}') = v(|\mathbf{q} + \mathbf{G}|) (\mathbf{q} + \mathbf{G}) \cdot (\mathbf{q} + \mathbf{G}') D(\mathbf{G} - \mathbf{G}'),$$

where $D(\mathbf{G})$ is the Fourier transform of $D(\mathbf{r})$.

For a given momentum \mathbf{q} the dielectric matrix is diagonalized by the same matrix U that diagonalizes M ,

$$\sum_{\mathbf{G}'} \epsilon(\mathbf{q} + \mathbf{G}, \mathbf{q} + \mathbf{G}') U_{\mathbf{G}', i} = U_{\mathbf{G}, i} \Lambda_i \quad (\text{A7})$$

where the eigenvalues $\{\Lambda_i\}$ are related with the eigenvalues of M , $\{\lambda_i\}$, through

$$\Lambda_i = 1 - \frac{\lambda_i}{\omega^2}. \quad (\text{A8})$$

Thus the frequencies of the **plasmon modes** are determined by the square roots of the eigenvalues of M .

The microscopic dielectric constant can be related to the observed macroscopic dielectric function $\bar{\epsilon}(\mathbf{q}, \omega)$ by

$$\bar{\epsilon}(\mathbf{q}, \omega) = \frac{1}{\left[(\epsilon(\mathbf{G}, \mathbf{G}'))^{-1} \right]_{\mathbf{G}=\mathbf{G}'=0}}.$$

A representative result for this quantity is shown in Fig. 1. Experimentally observable plasmons¹¹⁰ correspond to the zeros of $\bar{\epsilon}(\mathbf{q}, \omega)$. Numerically these appear at the maxima of

$$\text{Im} \left[(\epsilon(\mathbf{G}, \mathbf{G}'))^{-1} \right]_{\mathbf{G}=\mathbf{G}'=0} = \sum_i U_{\mathbf{G}=0, i} \frac{\eta \omega \lambda_i}{(\omega^2 - \lambda_i)^2 + \eta^2 \omega^2} U_{\mathbf{G}=0, i}.$$

where η is a quasiparticle lifetime broadening. Note that this last quantity can slightly shift the frequencies of the plasmons.

Appendix B: Zak Phase in Systems with Spatial Inversion Symmetry

The Zak phase is given by the expression

$$\gamma_n = i \int_{-\frac{\pi}{d}}^{\frac{\pi}{d}} dk \langle U_{n,k}(x) \sigma_z \partial_k U_{n,k}(x) \rangle \quad (\text{B1})$$

where $U_{n,k}(x)$ is the cell-periodic part of the Bloch wavefunction,

$$\Psi_{n,k}(x) = e^{ikx} U_{n,k}(x). \quad (\text{B2})$$

The Pauli matrix appears in the definition of the Zak phase because of the symplectic character of the Bogoliubov-Hopf transformation^{93,94}. Because the system is periodic, the inner product $\langle U_{n,k}(x) \sigma_z \partial_k U_{n,k}(x) \rangle$ involves an integration over a single unit cell. Then

$$\gamma_n = i \int_{-\frac{\pi}{d}}^{\frac{\pi}{d}} dk \langle \Psi_{n,k}^*(x) \sigma_z \partial_k \Psi_{n,k}(x) \rangle + \int_{-\frac{\pi}{d}}^{\frac{\pi}{d}} dk \langle \Psi_{n,k}(x) \sigma_z x \Psi_{n,k}(x) \rangle. \quad (\text{B3})$$

The origin of coordinates for the system is chosen at a center of inversion symmetry, and the last term is zero because of this. On the other hand systems with spatial inversion symmetry satisfy

$$\Psi_{n,k}(x) = e^{-i\phi_n(k)} \hat{\mathcal{I}} \Psi_{n,-k}(x), \quad (\text{B4})$$

where $\hat{\mathcal{I}}$ is the spatial inversion operator, and $\phi_n(k)$ is an arbitrary phase. Then

$$\begin{aligned} \gamma_n &= i \int_0^{\frac{\pi}{d}} dk \langle \Psi_{n,k}(x) \sigma_z \partial_k \Psi_{n,k}(x) \rangle + i \int_{-\frac{\pi}{d}}^0 dk \langle \Psi_{n,-k}(x) \hat{\mathcal{I}}^\dagger e^{-i\phi(k)} \sigma_z \partial_k e^{-i\phi_n(k)} \hat{\mathcal{I}} \Psi_{n,-k}(x) \rangle \\ &= i \int_0^{\frac{\pi}{d}} dk \langle \Psi_{n,k}(x) \sigma_z \partial_k \Psi_{n,k}(x) \rangle + i \int_{-\frac{\pi}{d}}^0 dk \langle \Psi_{n,-k}(x) \sigma_z \partial_k \Psi_{n,-k}(x) \rangle + \int_{-\frac{\pi}{d}}^0 dk \partial_k \phi_n(k) \\ &= i \int_0^{\frac{\pi}{d}} dk \langle \Psi_{n,k}(x) \sigma_z \partial_k \Psi_{n,k}(x) \rangle - i \int_{\frac{\pi}{d}}^0 dk \langle \Psi_{n,k}(x) \sigma_z \partial_{-k} \Psi_{n,k}(x) \rangle + \int_{-\frac{\pi}{d}}^0 dk \partial_k \phi_n(k) \\ &= i \int_0^{\frac{\pi}{d}} dk \langle \Psi_{n,k}(x) \sigma_z \partial_k \Psi_{n,k}(x) \rangle + i \int_0^{\frac{\pi}{d}} dk \langle \Psi_{n,k}(x) | \sigma_z \partial_{-k} \Psi_{n,k}(x) \rangle + \int_{-\frac{\pi}{d}}^0 dk \partial_k \phi_n(k) \\ &= i \int_0^{\frac{\pi}{d}} dk \langle \Psi_{n,k}(x) | \sigma_z \partial_k \Psi_{n,k}(x) \rangle - i \int_0^{\frac{\pi}{d}} dk \langle \Psi_{n,k}(x) | \sigma_z \partial_k \Psi_{n,k}(x) \rangle + \int_{-\frac{\pi}{d}}^0 dk \partial_k \phi_n(k) \\ &= \phi_n(0) - \phi(-\frac{\pi}{d}) = \phi_n(0) - \phi_n(-\frac{G_n}{2}) \end{aligned} \quad (\text{B5})$$

In the second line above we have used the normalization condition $\sum_{G_n} [(\alpha_{k+G_n}^n)^2 - (\beta_{k+G_n}^n)^2] = 1$.

In general the phase $\phi_n(k)$ can take any value for an arbitrary value of k . However, for a time reversal invariant momentum, k_T , which satisfies $k_T = -k_T + G_n$, the phase should obey

$$\Psi_{n,k_T} = e^{i\phi_n(k_T)} \hat{\mathcal{T}} \Psi_{n,k_T} = e^{i\phi_n(k_T)} \xi_n(k_T) \Psi_{n,k_T} \quad (\text{B6})$$

where $\xi_n(k)$ is the parity eigenvalue of the wavefunction at this wavevector.

Therefore, at time reversal invariant momentum points, the phase must take the **values 0 or π** . Specifically, if $\xi_n(k_T) = 1$, the phase is $\phi_n(k_T) = 0$, and if $\xi_n(k_T) = -1$ the phase is $\phi_n(k_T) = \pi$. Thus,

$$\gamma_n = \phi_n(0) - \phi(-\frac{\pi}{d}) = \begin{cases} 0 & \text{when states at } k = 0 \text{ and } k = G_0/2 \text{ have the same symmetry} \\ \pi & \text{when states at } k = 0 \text{ and } k = G_0/2 \text{ have opposite symmetry} \end{cases}. \quad (\text{B7})$$

This leads to the final result

$$e^{i\gamma_n} = \xi_n(k=0) \xi_n(k=\frac{G_0}{2}) \quad (\text{B8})$$

which is presented as Eq. 16 in the main text.

-
- ¹ David Pines and David Bohm, “A collective description of electron interactions: Ii. collective $\mathcal{M}\{\text{vs}\}$ individual particle aspects of the interactions,” *Physical Review* **85**, 338–353 (1952).
 - ² David Pines, “Collective energy losses in solids,” *Reviews of Modern Physics* **28**, 184–198 (1956).
 - ³ K. Sawada, K. A. Brueckner, N. Fukuda, and R. Brout, “Correlation energy of an electron gas at high density: Plasma oscillations,” *Physical Review* **108**, 507–514 (1957).
 - ⁴ G. Giuliani and G. Vignale, *Quantum Theory of the Electron Liquid* (Cambridge University Press, 2005).
 - ⁵ J M Pitarke, V M Silkin, E V Chulkov, and P M Echenique, “Theory of surface plasmons and surface-plasmon polaritons,” *Reports on Progress in Physics* **70**, 1 (2007).
 - ⁶ R. H. Ritchie, “Plasma losses by fast electrons in thin films,” *Physical Review* **106**, 874–881 (1957).
 - ⁷ Tsuneya Ando, Alan B. Fowler, and Frank Stern, “Electronic properties of two-dimensional systems,” *Reviews of Modern Physics* **54**, 437–672 (1982).
 - ⁸ Tobias Stauber, “Plasmonics in dirac systems: from graphene to topological insulators,” *J. Phys.: Condens. Matter* **26**, 123201 (2014).
 - ⁹ T. Stauber, G. Gómez-Santos, and L. Brey, “Spin-charge separation of plasmonic excitations in thin topological insulators,” *Physical Review B* **88**, 205427– (2013).
 - ¹⁰ Tobias Stauber, Guillermo Gómez-Santos, and Luis Brey, “Plasmonics in topological insulators: Spin-charge separation, the influence of the inversion layer, and phonon-plasmon coupling,” *ACS Photonics* **4**, 2978–2988 (2017).
 - ¹¹ A.Y. Nikitin, *Graphene Plasmonics*, World Scientific Handbook of Metamaterials and Plasmonics, Vol. 1 (World Scientific Publishing, 2017).
 - ¹² A. Yu. Nikitin, F. Guinea, F. J. García-Vidal, and L. Martín-Moreno, “Edge and waveguide terahertz surface plasmon modes in graphene microribbons,” *Physical Review B* **84**, 161407– (2011).
 - ¹³ Frank H. L. Koppens, Darrick E. Chang, and F. Javier García de Abajo, “Graphene plasmonics: A platform for strong light–matter interactions,” *Nano Letters*, *Nano Letters* **11**, 3370–3377 (2011).
 - ¹⁴ T M Slipchenko, M L Nesterov, L Martin-Moreno, and A Yu Nikitin, “Analytical solution for the diffraction of an electromagnetic wave by a graphene grating,” *Journal of Optics* **15**, 114008 (2013).
 - ¹⁵ P.A.D. Goncalves and N.M.R. Peres, *An Introduction to Graphene Plasmonics* (World Scientific, Singapur, 2016).
 - ¹⁶ A. Gonzalez-Tudela, D. Martin-Cano, E. Moreno, L. Martin-Moreno, C. Tejedor, and F. J. Garcia-Vidal, “Entanglement of two qubits mediated by one-dimensional plasmonic waveguides,” *Physical Review Letters* **106**, 020501– (2011).
 - ¹⁷ P Törmä and W L Barnes, “Strong coupling between surface plasmon polaritons and emitters: a review,” *Reports on Progress in Physics*, *Reports on Progress in Physics* **78**, 013901 (2015).
 - ¹⁸ A. González-Tudela, P. A. Huidobro, L. Martín-Moreno, C. Tejedor, and F. J. García-Vidal, “Theory of strong coupling between quantum emitters and propagating surface plasmons,” *Physical Review Letters* **110**, 126801– (2013).
 - ¹⁹ Jacopo Fregoni, Francisco J. Garcia-Vidal, and Johannes Feist, “Theoretical challenges in polaritonic chemistry,” *ACS Photonics*, *ACS Photonics* **9**, 1096–1107 (2022).
 - ²⁰ Marinko Jablan, Hrvoje Buljan, and Marin Soljačić, “Plasmonics in graphene at infrared frequencies,” *Physical Review B* **80**, 245435– (2009).
 - ²¹ A. N. Grigorenko, M. Polini, and K. S. Novoselov, “Graphene plasmonics,” *Nature Photonics* **6**, 749–758 (2012).
 - ²² Z. Fei, A. S. Rodin, G. O. Andreev, W. Bao, A. S. McLeod, M. Wagner, L. M. Zhang, Z. Zhao, M. Thieme, G. Dominguez, M. M. Fogler, A. H. Castro Neto, C. N. Lau, F. Keilmann, and D. N. Basov, “Gate-tuning of graphene plasmons revealed by infrared nano-imaging,” *Nature* **487**, 82–85 (2012).
 - ²³ Jianing Chen, Michela Badioli, Pablo Alonso-González,

- Sukosin Thongrattanasiri, Florian Huth, Johann Osmond, Marko Spasenović, Alba Centeno, Amaia Pesquera, Philippe Godignon, Amaia Zurutuza Elorza, Nicolas Camara, F. Javier García de Abajo, Rainer Hillenbrand, and Frank H. L. Koppens, “Optical nano-imaging of gate-tunable graphene plasmons,” *Nature* **487**, 77–81 (2012).
- ²⁴ Z. Fei, A. S. Rodin, G. O. Andreev, W. Bao, A. S. McLeod, M. Wagner, L. M. Zhang, Z. Zhao, M. Thiemens, G. Dominguez, M. M. Fogler, A. H. Castro Neto, C. N. Lau, F. Keilmann, and D. N. Basov, “Gate-tuning of graphene plasmons revealed by infrared nano-imaging,” *Nature* **487**, 82–85 (2012).
- ²⁵ Z. Fei, A. S. Rodin, W. Gannett, S. Dai, W. Regan, M. Wagner, M. K. Liu, A. S. McLeod, G. Dominguez, M. Thiemens, Antonio H. Castro Neto, F. Keilmann, A. Zettl, R. Hillenbrand, M. M. Fogler, and D. N. Basov, “Electronic and plasmonic phenomena at graphene grain boundaries,” *Nature Nanotechnology* **8**, 821–825 (2013).
- ²⁶ Achim Woessner, Mark B. Lundberg, Yuanda Gao, Alessandro Principi, Pablo Alonso-González, Matteo Carrega, Kenji Watanabe, Takashi Taniguchi, Giovanni Vignale, Marco Polini, James Hone, Rainer Hillenbrand, and Frank H. L. Koppens, “Highly confined low-loss plasmons in graphene–boron nitride heterostructures,” *Nature Materials* **14**, 421–425 (2015).
- ²⁷ A. Yu. Nikitin, F. Guinea, F. J. Garcia-Vidal, and L. Martin-Moreno, “Surface plasmon enhanced absorption and suppressed transmission in periodic arrays of graphene ribbons,” *Physical Review B* **85**, 081405– (2012).
- ²⁸ Bo Zhao and Zhuomin M. Zhang, “Strong plasmonic coupling between graphene ribbon array and metal gratings,” *ACS Photonics*, *ACS Photonics* **2**, 1611–1618 (2015).
- ²⁹ Eduardo J. C. Dias and N. M. R. Peres, “Controlling spoof plasmons in a metal grating using graphene surface plasmons,” *ACS Photonics*, *ACS Photonics* **4**, 3071–3080 (2017).
- ³⁰ Tatiana G. Rappoport, Yuliy V. Bludov, Frank H. L. Koppens, and Nuno M. R. Peres, “Topological graphene plasmons in a plasmonic realization of the su–schrieffer–heeger model,” *ACS Photonics*, *ACS Photonics* **8**, 1817–1823 (2021).
- ³¹ Tianjing Guo and Christos Argyropoulos, “Hybrid graphene-plasmon gratings,” *Journal of Applied Physics* **134**, 050901 (2023).
- ³² A. V. Nikonov, A. A. Zabolotnykh, and V. A. Volkov, “Plasmons in two-dimensional electron systems with infinite and semi-infinite metal gratings,” (2024), arXiv:2406.12579 [cond-mat.mes-hall].
- ³³ Long Ju, Baisong Geng, Jason Horng, Caglar Girit, Michael Martin, Zhao Hao, Hans A. Bechtel, Xiaogan Liang, Alex Zettl, Y. Ron Shen, and Feng Wang, “Graphene plasmonics for tunable terahertz metamaterials,” *Nature Nanotechnology* **6**, 630–634 (2011).
- ³⁴ Jared H. Strait, Parinita Nene, Wei-Min Chan, Christina Manolatu, Sandip Tiwari, Farhan Rana, Joshua W. Kevek, and Paul L. McEuen, “Confined plasmons in graphene microstructures: Experiments and theory,” *Physical Review B* **87**, 241410– (2013).
- ³⁵ Andrey Bylinkin, Elena Titova, Vitaly Mikheev, Elena Zhukova, Sergey Zhukov, Mikhail Belyanchikov, Mikhail Kashchenko, Andrew Miakonkikh, and Dmitry Svitsov, “Tight-binding terahertz plasmons in chemical-vapor-deposited graphene,” *Physical Review Applied* **11**, 054017– (2019).
- ³⁶ Dafei Jin, Thomas Christensen, Marin Soljačić, Nicholas X. Fang, Ling Lu, and Xiang Zhang, “Infrared topological plasmons in graphene,” *Physical Review Letters* **118**, 245301– (2017).
- ³⁷ Milad Taleb Hesami Azar, Mahdi Zavvari, Yashar Zehforoosh, and Pejman Mohammadi, “Graphene plasmonic crystal: Two-dimensional gate-controlled chemical potential for creation of photonic bandgap,” *Plasmonics* **15**, 975–983 (2020).
- ³⁸ L. Xiong, C. Forsythe, M. Jung, A. S. McLeod, S. S. Sunku, Y. M. Shao, G. X. Ni, A. J. Sternbach, S. Liu, J. H. Edgar, E. J. Mele, M. M. Fogler, G. Shvets, C. R. Dean, and D. N. Basov, “Photonic crystal for graphene plasmons,” *Nature Communications* **10**, 4780 (2019).
- ³⁹ John D. Joannopoulos, Steven G. Johnson, Joshua N. Winn, and Robert D. Meade, *Photonic Crystals: Molding the Flow of Light (Second Edition)*, 2nd ed. (Princeton University Press, 2008).
- ⁴⁰ David Vanderbilt, *Berry Phases in Electronic Structure Theory: Electric Polarization, Orbital Magnetization and Topological Insulators* (Cambridge University Press, Cambridge, 2018).
- ⁴¹ R. Guo, T. K. Hakala, and P. Törmä, “Geometry dependence of surface lattice resonances in plasmonic nanoparticle arrays,” *Physical Review B* **95**, 155423– (2017).
- ⁴² Javier Cuerda, Jani M. Taskinen, Nicki Källman, Leo Grabitz, and Päivi Törmä, “Pseudospin-orbit coupling and non-hermitian effects in the quantum geometric tensor of a plasmonic lattice,” *Physical Review B* **109**, 165439– (2024).
- ⁴³ Javier Cuerda, Jani M. Taskinen, Nicki Källman, Leo Grabitz, and Päivi Törmä, “Observation of quantum metric and non-hermitian berry curvature in a plasmonic lattice,” *Physical Review Research* **6**, L022020– (2024).
- ⁴⁴ Zhihao Lan, Menglin L. N. Chen, Fei Gao, Shuang Zhang, and Wei E. I. Sha, “A brief review of topological photonics in one, two, and three dimensions,” *Reviews in Physics* **9**, 100076 (2022).
- ⁴⁵ Long-Hua Wu and Xiao Hu, “Scheme for achieving a topological photonic crystal by using dielectric material,” *Physical Review Letters* **114**, 223901– (2015).
- ⁴⁶ S. F. Mingaleev and Y. S. Kivshar, “Nonlinear localized modes in 2d photonic crystals and waveguides,” in *Nonlinear Photonic Crystals*, edited by Richard E. Slusher and Benjamin J. Eggleton (Springer Berlin Heidelberg, Berlin, Heidelberg, 2003) pp. 351–369.
- ⁴⁷ Vaibhav Gupta and Barry Bradlyn, “Wannier-function methods for topological modes in one-dimensional photonic crystals,” *Physical Review A* **105**, 053521– (2022).
- ⁴⁸ Luis Brey, T. Stauber, L. Martín-Moreno, and G. Gómez-Santos, “Nonlocal quantum effects in plasmons of graphene superlattices,” *Physical Review Letters* **124**, 257401– (2020).
- ⁴⁹ R. De L. Kronig, William George Penney, and Ralph Howard Fowler, “Quantum mechanics of electrons in crystal lattices,” *Proceedings of the Royal Society of London. Series A, Containing Papers of a Mathematical and Physical Character*, Proceedings of the Royal Society of London. Series A, Containing Papers of a Mathematical and Physical Character **130**, 499–513 (1997).
- ⁵⁰ W. P. Su, J. R. Schrieffer, and A. J. Heeger, “Solitons in polyacetylene,” *Physical Review Letters* **42**, 1698–1701

- (1979).
- ⁵¹ Tatiana G. Rappoport, Yuliy V. Bludov, Frank H. L. Koppens, and Nuno M. R. Peres, “Topological graphene plasmons in a plasmonic realization of the su–schrieffer–heeger model,” *ACS Photonics*, ACS Photonics **8**, 1817–1823 (2021).
 - ⁵² C. Liu and H. C. Ong, “Realization of topological superlattices and the associated interface states in one-dimensional plasmonic crystals,” *Physical Review B* **106**, 045401– (2022).
 - ⁵³ Thomas Benjamin Smith, Coskun Kocabas, and Alessandro Principi, “Topological plasmonic waveguides in triharmonic metal gratings,” *Journal of Physics: Condensed Matter*, **33**, 265003 (2021).
 - ⁵⁴ D. A. Miranda, Y. V. Bludov, N. Asger Mortensen, and N. M. R. Peres, “Topology in a one-dimensional plasmonic crystal,” (2024), arXiv:2404.19576 [cond-mat.mes-hall].
 - ⁵⁵ F. B. Pedersen, G. T. Einevoll, and P. C. Hemmer, “Wannier functions for the kronig-penney model,” *Physical Review B* **44**, 5470–5475 (1991).
 - ⁵⁶ Vaibhav Gupta and Barry Bradlyn, “Wannier-function methods for topological modes in one-dimensional photonic crystals,” *Physical Review A* **105**, 053521– (2022).
 - ⁵⁷ B Wunsch, T Stauber, F Sols, and F Guinea, “Dynamical polarization of graphene at finite doping,” *New Journal of Physics* **8**, 318–318 (2006).
 - ⁵⁸ E. H. Hwang and S. Das Sarma, “Dielectric function, screening, and plasmons in two-dimensional graphene,” *Physical Review B* **75**, 205418– (2007).
 - ⁵⁹ L. Brey and H. A. Fertig, “Elementary electronic excitations in graphene nanoribbons,” *Physical Review B* **75**, 125434– (2007).
 - ⁶⁰ A. H. Castro Neto, F. Guinea, N. M. R. Peres, K. S. Novoselov, and A. K. Geim, “The electronic properties of graphene,” *Rev. Mod. Phys.* **81**, 109–162 (2009).
 - ⁶¹ M.I.Katsnelson, *Graphene* (Cambridge, 2012).
 - ⁶² J. M. Elson and R. H. Ritchie, “Photon interactions at a rough metal surface,” *Physical Review B* **4**, 4129–4138 (1971).
 - ⁶³ T. Gruner and D. G. Welsch, “Green-function approach to the radiation-field quantization for homogeneous and inhomogeneous kramers-kronig dielectrics,” *Physical Review A* **53**, 1818–1829 (1996).
 - ⁶⁴ Alexandre Archambault, François Marquier, Jean-Jacques Greffet, and Christophe Arnold, “Quantum theory of spontaneous and stimulated emission of surface plasmons,” *Physical Review B* **82**, 035411– (2010).
 - ⁶⁵ George W. Hanson, S. A. Hassani Gangaraj, Changhyoup Lee, Dimitris G. Angelakis, and Mark Tame, “Quantum plasmonic excitation in graphene and loss-insensitive propagation,” *Physical Review A* **92**, 013828– (2015).
 - ⁶⁶ Beatriz A. Ferreira, B. Amorim, A. J. Chaves, and N. M. R. Peres, “Quantization of graphene plasmons,” *Physical Review A* **101**, 033817– (2020).
 - ⁶⁷ Luis Brey and H. A. Fertig, “Quantum plasmons in double layer systems,” *Physical Review B* **109**, 045303– (2024).
 - ⁶⁸ N M R Peres, Aires Ferreira, Yu V Bludov, and M I Vasilevskiy, “Light scattering by a medium with a spatially modulated optical conductivity: the case of graphene,” *Journal of Physics: Condensed Matter* **24**, 245303 (2012).
 - ⁶⁹ I Silveiro, A Manjavacas, S Thongrattanasiri, and F J García de Abajo, “Plasmonic energy transfer in periodically doped graphene,” *New Journal of Physics* **15**, 033042 (2013).
 - ⁷⁰ Chris Beckerleg and Euan Hendry, “Localized plasmons induced by spatial conductivity modulation in graphene,” *Journal of the Optical Society of America B* **33**, 2051–2056 (2016).
 - ⁷¹ Paloma A. Huidobro, Matthias Kraft, Stefan A. Maier, and John B. Pendry, “Graphene as a tunable anisotropic or isotropic plasmonic metasurface,” *ACS Nano* **10**, 5499–5506 (2016).
 - ⁷² P A Huidobro, M Kraft, R Kun, S A Maier, and J B Pendry, “Graphene, plasmons and transformation optics,” *Journal of Optics* **18**, 044024 (2016).
 - ⁷³ L. Brey and H. A. Fertig, “Linear response and the thomas-fermi approximation in undoped graphene,” *Physical Review B* **80**, 035406– (2009).
 - ⁷⁴ C. Fabre G. Gilbert, A. Aspect, *Introduction to Quantum Optics* (Cambridge University Press, 2010).
 - ⁷⁵ W. Vogel and D-G Welsch, *Quantum Optics* (Wiley, 2006).
 - ⁷⁶ Guillaume Malpuech Alexey V. Kavokin, Jeremy J. Baumberg and Fabrice P. Laussy, *Microcavities* (Oxford University Press, 2007).
 - ⁷⁷ Anton Frisk Kockum, Adam Miranowicz, Simone De Liberato, Salvatore Savasta, and Franco Nori, “Ultrastrong coupling between light and matter,” *Nature Reviews Physics* **1**, 19–40 (2019).
 - ⁷⁸ Peter Kirton, Mor M. Roses, Jonathan Keeling, and Emanuele G. Dalla Torre, “Introduction to the dicke model: From equilibrium to nonequilibrium, and vice versa,” *Advanced Quantum Technologies*, Advanced Quantum Technologies **2**, 1800043 (2019).
 - ⁷⁹ Edward A. Sziklas, “Collective oscillations in a dense electron gas containing a fixed point charge,” *Physical Review* **138**, A1070–A1082 (1965).
 - ⁸⁰ S. Rudin and T. L. Reinecke, “Plasmons localized at point charges in semiconductor quantum wells,” *Physical Review B* **48**, 2223–2235 (1993).
 - ⁸¹ Iacopo Torre, Mikhail I. Katsnelson, Alberto Diaspro, Vittorio Pellegrini, and Marco Polini, “Lippmannschwinger theory for two-dimensional plasmon scattering,” *Physical Review B* **96**, 035433– (2017).
 - ⁸² Jinlyu Cao, H. A. Fertig, and Luis Brey, “Quantum internal structure of plasmons,” *Physical Review Letters* **127**, 196403– (2021).
 - ⁸³ The square root of the product of the coupled plasmon energies causes the potential, Eq.(7), to decrease with the reciprocal lattice vectors at a slower rate than the Fourier components of the Drude weight.
 - ⁸⁴ J.M.Ziman, *Elements of Advanced Quantum Theory* (Cambridge University Press, 1969).
 - ⁸⁵ J. J. Hopfield, “Theory of the contribution of excitons to the complex dielectric constant of crystals,” *Physical Review* **112**, 1555–1567 (1958).
 - ⁸⁶ Cristiano Ciuti, Gérald Bastard, and Iacopo Carusotto, “Quantum vacuum properties of the intersubband cavity polariton field,” *Physical Review B* **72**, 115303– (2005).
 - ⁸⁷ Walter A. Harrison, *Electronic Structure and the Properties of Solids* (Dover books on Physics, 1989).
 - ⁸⁸ Neil W. Ascroft and N.David Mermin, *Solid State Physics* (Saunders College Publishing, 1976).
 - ⁸⁹ Peter Y. Yu and Manuel Cardona, *Fundamentals of Semiconductors* (Springer, 1996).
 - ⁹⁰ Di Xiao, Ming-Che Chang, and Qian Niu, “Berry phase effects on electronic properties,” *Rev. Mod. Phys.* **82**,

- 1959–2007 (2010).
- ⁹¹ J. Zak, “Band center—a conserved quantity in solids,” *Physical Review Letters* **48**, 359–362 (1982).
 - ⁹² J. Zak, “Berry’s phase for energy bands in solids,” *Phys. Rev. Lett.* **62**, 2747–2750 (1989).
 - ⁹³ Ryuichi Shindou, Ryo Matsumoto, Shuichi Murakami, and Jun-ichiro Ohe, “Topological chiral magnonic edge mode in a magnonic crystal,” *Physical Review B* **87**, 174427– (2013).
 - ⁹⁴ Tal Goren, Kirill Plekhanov, Félicien Appas, and Karyn Le Hur, “Topological zak phase in strongly coupled lc circuits,” *Physical Review B* **97**, 041106– (2018).
 - ⁹⁵ Liang Fu and C. L. Kane, “Topological insulators with inversion symmetry,” *Physical Review B* **76**, 045302– (2007).
 - ⁹⁶ Taylor L. Hughes, Emil Prodan, and B. Andrei Bernevig, “Inversion-symmetric topological insulators,” *Physical Review B* **83**, 245132– (2011).
 - ⁹⁷ Guido van Miert, Carmine Ortix, and Cristiane Morais Smith, “Topological origin of edge states in two-dimensional inversion-symmetric insulators and semimetals,” *2D Materials*, *2D Materials* **4**, 015023 (2017).
 - ⁹⁸ Liang Fu and C. L. Kane, “Time reversal polarization and a \mathbb{Z}_2 adiabatic spin pump,” *Physical Review B* **74**, 195312– (2006).
 - ⁹⁹ R. Jackiw and C. Rebbi, “Solitons with fermion number $\frac{1}{2}$,” *Physical Review D* **13**, 3398–3409 (1976).
 - ¹⁰⁰ A. J. Heeger, S. Kivelson, J. R. Schrieffer, and W. P. Su, “Solitons in conducting polymers,” *Reviews of Modern Physics* **60**, 781–850 (1988).
 - ¹⁰¹ M. Z. Hasan and C. L. Kane, “Colloquium: Topological insulators,” *Reviews of Modern Physics* **82**, 3045–3067 (2010).
 - ¹⁰² J Cayssol and J N Fuchs, “Topological and geometrical aspects of band theory,” *Journal of Physics: Materials*, *Journal of Physics: Materials* **4**, 034007 (2021).
 - ¹⁰³ Carlos G. Velasco and Belén Paredes, “Realizing and detecting a topological insulator in the aiii symmetry class,” *Physical Review Letters* **119**, 115301– (2017).
 - ¹⁰⁴ Edward McCann, “Catalog of noninteracting tight-binding models with two energy bands in one dimension,” *Physical Review B* **107**, 245401– (2023).
 - ¹⁰⁵ Beatriz Pérez-González, Miguel Bello, Álvaro Gómez-León, and Gloria Platero, “Interplay between long-range hopping and disorder in topological systems,” *Physical Review B* **99**, 035146– (2019).
 - ¹⁰⁶ Eric J. Meier, Fangzhao Alex An, Alexandre Dauphin, Maria Maffei, Pietro Massignan, Taylor L. Hughes, and Bryce Gadway, “Observation of the topological anderson insulator in disordered atomic wires,” *Science*, *Science* **362**, 929–933 (2018).
 - ¹⁰⁷ M. Kiczynski, S. K. Gorman, H. Geng, M. B. Donnelly, Y. Chung, Y. He, J. G. Keizer, and M. Y. Simmons, “Engineering topological states in atom-based semiconductor quantum dots,” *Nature* **606**, 694–699 (2022).
 - ¹⁰⁸ Marcos Atala, Monika Aidelsburger, Julio T. Barreiro, Dmitry Abanin, Takuya Kitagawa, Eugene Demler, and Immanuel Bloch, “Direct measurement of the zak phase in topological bloch bands,” *Nature Physics* **9**, 795–800 (2013).
 - ¹⁰⁹ N. R. Cooper, J. Dalibard, and I. B. Spielman, “Topological bands for ultracold atoms,” *Reviews of Modern Physics* **91**, 015005– (2019).
 - ¹¹⁰ M. Pizarra, A. Sindona, M. Gravina, V. M. Silkin, and J. M. Pitarke, “Dielectric screening and plasmon resonances in bilayer graphene,” *Physical Review B* **93**, 035440– (2016).